

NUMERICAL SIMULATIONS OF TRANSVERSE COMPRESSION AND DENSIFICATION IN WOOD

*John A. Nairn*¹

Professor
Material Science and Engineering
University of Utah
Salt Lake City, UT 84112

(Received February 2005)

ABSTRACT

Numerical modeling, such as finite element analysis (FEA), of complex structures and complex materials is a useful tool for stress analysis and for failure modeling. Although FEA of wood as an anisotropic continuum is used, numerical modeling of realistic wood structures, including details of wood anatomy and variations in structure within specimens, has been beyond the capabilities of FEA and other methods. In contrast, the recently derived material point method (MPM) has features that make it amenable to analysis of realistic wood structures. To demonstrate the capabilities of MPM, simulations were done for wood in transverse compression. Some advantages of MPM are that it is easy to discretize micrographs of wood specimens into a numerical model, it can handle large deformations, it can model elastic-plastic cell-wall properties, and it automatically accounts for contact between cell walls. MPM simulations were run for softwood and hardwood loaded in either radial or tangential compression. The simulations reproduced many features of wood compression, gave insight into effects of wood anatomy on compression, and may be the first numerical calculations of realistic wood structures extended through to full densification without numerical difficulties.

Keywords: Wood, compression, material point method, numerical modeling, plastic collapse, densification.

INTRODUCTION

Figure 1 shows three regions during quasi-static, transverse compression of wood (Bodig 1963, 1965, 1966). At low strain, the deformation is linear and elastic. This region ends in a collapse region of relatively constant stress. The collapse is initiated by elastic or plastic buckling of cell walls or by fracture of cell walls. At very high strains, the collapsed cell walls contact other cell walls, and the stress increases rapidly during wood densification. Although all wood exhibits these general features, key details of compression properties are dependent on various anatomical features of the wood specimen such as density, percentage of latewood material, ray volume, etc., and on loading direction with respect to radial and tangential directions (Bodig

1963, 1965, 1966; Kennedy 1968; Kunesh 1968; Gibson et al. 1981; Easterling et al. 1982). The goal of this paper is to demonstrate a numerical method that can address details about the effect of wood anatomy on the transverse compression and densification of wood. Results on compression of wood are relevant to wood in structural design and in processing of wood-based composites (Bodig and Jayne 1982).

Gibson and Ashby (Gibson et al. 1982; Gibson and Ashby 1997) derived analytical models for 2D foams that are approximately applicable to analysis of wood (Gibson et al. 1981; Easterling et al. 1982). These models describe a foam (or wood) structure as a regular array of hexagonal cells (see Fig. 1 insert) and derive results for initial elastic modulus and initiation of failure by either elastic or plastic buckling. These models capture the essential mechanisms of wood failure, and have been useful for interpreting compression experiments on wood (Tabarsa 1999;

¹ Current address: John A. Nairn, Professor and Richardson Chair, Wood Science and Engineering, Oregon State University, Corvallis, OR 97331

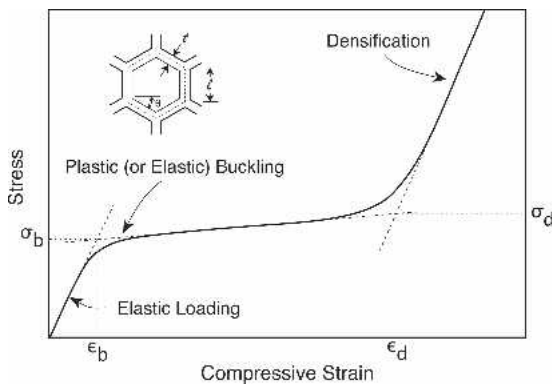


FIG. 1. Schematic view of a transverse compression stress-strain curve for wood. The dotted lines show the method used to extract initial modulus (E), stress and strain for the onset of buckling (σ_b and ϵ_b) and the stress and strain for the onset of densification (σ_d and ϵ_d). The insert shows a piece of a regular hexagonal array.

Tabarsa and Chui 2000, 2001). Analytical foam models, however, are limited to low-density foams ($t/l \ll 1$ for which the mechanisms modeled dominate the deformation) and can not be extended into wood densification. Furthermore, any model, analytical or numerical, that uses a regular array of cells can not handle effects of variations in cell structure due to wood anatomy. Work on these problems requires numerical modeling of realistic wood structures.

Finite element analysis (FEA) is a common method for numerical modeling of structures, but there are at least four reasons FEA has difficulty modeling realistic wood specimens (Bardenhagen et al. 2005). First, the structure of wood is complex. It is very difficult to discretize such structures into an FEA mesh. The common FEA practice of reducing analysis to a small idealized structure limits its value for numerical modeling of the details or failure mechanisms (Smith et al. 2003). Second, the densification of wood involves contact between cell walls. Although contact methods are available in FEA, they are not fully developed for analysis of arbitrary contact. Furthermore, it would be difficult to mesh contact elements within realistic structures. Third, buckling of walls and subsequent densification requires large deformations. The elements in an FEA mesh would become

too distorted at high strains and numerical problems would occur. Fourth, the number of elements required to accurately mesh realistic wood morphology is computationally expensive (Smith et al. 2003).

To date, FEA work on wood compression has been limited to specialized problems and no work has considered densification of wood. For example, Pellicane et al. (1994a, 1994b) used continuum FEA to model an ASTM specimen for transverse compression. The model was for a linear elastic, isotropic material and did not attempt to consider any details of wood structure. Recently, Shiari (Shiari and Wild 2004) used FEA to consider compression including large deformations and contact. This analysis, however, was limited to a single wood cell and only considered linear elastic material properties. Analogously, FEA results on foams have focused on modest deformation and idealized meshes (Zhu et al. 1997).

Recently, lattice methods have been suggested as a potential morphology-based tool in which the wood structure is replaced by a model of rod and spring elements (Smith et al. 2003; Landis et al. 2002; Davids et al. 2003). The hope is that lattice models may be more efficient than FEA analysis and be able to describe realistic wood structures. To date, however, lattice models have resorted to regular arrays of springs and rods and have been limited to linear elastic material properties. Variations in wood structure have been introduced by allowing strength and/or stiffness properties of the elements to be statistical quantities. The choice of statistical parameters, however, while guided by experimental results, must include some *ad hoc* assumptions (Landis et al. 2002). Lattice models have focused on longitudinal properties of wood where the rods are wood fibers and springs represent transverse properties (Landis et al. 2002; Davids et al. 2003). In principle, lattice models could be applied to transverse properties or 3D modeling, but that capability has not been demonstrated.

The goal of this paper is to develop the material point method (MPM) as a potential tool for numerical modeling of wood that is capable of

modeling many details of wood anatomy. The idea for use of MPM on wood was derived from the recent successful application of MPM to 3D foams (Bardenhagen et al. 2005; Brydon et al. 2005). Those results showed that prior problems associated with numerical modeling of foam (or wood) are either absent or less severe when using MPM (Bardenhagen et al. 2005). First, it is very easy to discretize realistic structures in MPM. The process is analogous to digitization of an image into pixels. Second, MPM automatically handles contact and thus can be extended to high strain or densification without numerical difficulty. Third, MPM can handle realistic material models and large deformations. Fourth, as the results presented here demonstrate, MPM can handle large calculations.

The NUMERICAL METHODS section briefly describes the material point method (MPM) and the discretization of micrographs of real wood into a numerical model. The RESULTS AND DISCUSSION section describes MPM simulations of compression on loblolly pine, yellow poplar, and ponderosa pine. The results include compression in the radial and tangential directions, compression of softwood vs. hardwood, the effect of cell-wall properties, and the effect of loading rate. The simulations reproduced many features of wood compression (see Fig. 1) and may be the first numerical calculations that extended through to full densification (the calculations were extended to 60% compressive strain). The results are compared to foam-theory models. The emphasis of this paper is on demonstration of MPM numerical capabilities for analysis of wood in compression. The CONCLUSIONS AND FUTURE WORK section suggests potential applications for MPM modeling as a general tool for analysis of wood including future direct comparisons between numerical modeling and experiments.

NUMERICAL METHODS

Material point method

The material point method (MPM) has been developed as a numerical method for solving problems in dynamic solid mechanics (Sulsky et

al. 1994, 1995; Sulsky and Schreyer 1996; Zhou 1998). In MPM, a solid body is discretized into a collection of points much as a computer image is represented by pixels. As the dynamic analysis proceeds, the solution is tracked on the material points by updating all required properties such as position, velocity, acceleration, stress state, etc. At each time step, the particle information is extrapolated to a background grid, which serves as a calculational tool to solve the equations of motion. Once the equations are solved, the grid-based solution is used to update all particle properties. This combination of Lagrangian and Eulerian methods has proven useful for solving solid mechanics problems including those with large deformations or rotations and involving materials with history-dependent properties such as plasticity or viscoelasticity effects (Sulsky et al. 1994). MPM is amenable to parallel computation (Parker 2002), implicit integration methods (Guilkey and Weiss 2003), and generalized interpolation schemes that can optimize accuracy (Bardenhagen and Kober 2004). MPM also has advantages for dealing with explicit cracks and crack propagation (Nairn 2003; Guo and Nairn 2004) and for analyses involving coupled thermal conductivity or moisture diffusion (Nairn 2005b).

Although MPM uses a background grid and is frequently compared to finite element methods, a new derivation of MPM (Bardenhagen and Kober 2004) presents it as a Petrov-Galerkin method that has similarities with meshless methods such as Element-Free Galerkin (EFG) methods (Belytschko et al. 1994) and Meshless-Local Petrov-Galerkin (MLPG) methods (Atluri and Shen 2002). The "meshless" aspect of MPM, despite the use of a grid, derives from the fact that the body and the solution are described on the particles while the grid is used solely for calculations. The meshless features of MPM have advantages for simulation of transverse compression in wood. First, it is easy to discretize actual wood anatomy simply by translation of pixels in a computer image of a wood micrographs into an MPM model for wood. Second, MPM can handle large deformations and large compression strains without any mesh dis-

tortion. The particles translate through the mesh, but the grid never changes and hence never distorts. Third, MPM automatically handles contact between particles and thus automatically handles cell-wall contact at high compressive strain during wood densification.

Numerical analysis of wood

Figure 2A shows an SEM micrograph of uncompresssed mature loblolly pine (*Pinus taeda*) (Kultikova 1999). The resolution of the image, as obtained, was 360×234 pixels and it images an area of 0.832×0.541 mm. To analyze this wood anatomy in MPM, the image was converted into a 256 level grayscale bitmap image (a standard, uncompressed, BMP file (Bourke 2004)). Next, an MPM background mesh was defined with any number of regular, quadrilat-

eral elements covering an area greater than or equal to the image area. Each element in the mesh was assigned to have four possible locations for material points each representing one quarter of the element area. Our 2D MPM code (Nairn 2005a) was then revised to map the BMP image to the mesh and evaluate the intensity of the image corresponding to each potential material point location. Based on the average image intensity, each location was either assigned to have a material point representing cell-wall material or to be vacant representing cell lumen or other open space. For the image in Fig. 2A, cell-wall material was identified with intensity 150 or greater (within a gray scale from 0 for black to 255 for white). The resolution of the MPM discretization could be adjusted arbitrarily to vary accuracy of digitizing the image. The result in Fig. 2B is an MPM model using a background grid for the image of 150×97 elements. This background grid provides for $300 \times 194 = 58,020$ potential locations for particles. The individual material points in Fig. 2B are drawn as square blocks, but are barely distinguishable. The background grid was omitted for clarity.

Individual cell walls are layered structures, but the layers are beyond the resolution of these calculations. Here cell-wall material was treated as a transversely isotropic continuum with the unique axis in the axial direction having a high modulus while the two directions in the transverse plane have equal moduli. Typical results for transverse-plane cell-wall modulus are around 10 GPa (Easterling et al. 1982). Recently, Tabarsa extracted transverse cell properties by experiments coupled with analysis of the cell anatomy of particular specimens (Tabarsa 1999; Tabarsa and Chui 2000, 2001). The results were 10.2–10.6 GPa for white spruce and 10.3 GPa for jack pine. All calculations in this paper assumed cell-wall properties with a transverse modulus of $E_w = 10.6$ GPa, a Poisson's ratio of $\nu = 0.33$, and a density of $\rho_w = 1500$ kg/m³ (Easterling et al. 1982). Using this cell-wall density, the bulk density of the digitized MPM model in Fig. 2B is 910 kg/m³ (35,352 particles or $\rho/\rho_w = 0.607$) varying from 605 kg/m³ ($\rho/\rho_w = 0.404$) in the earlywood region to 1186 kg/m³

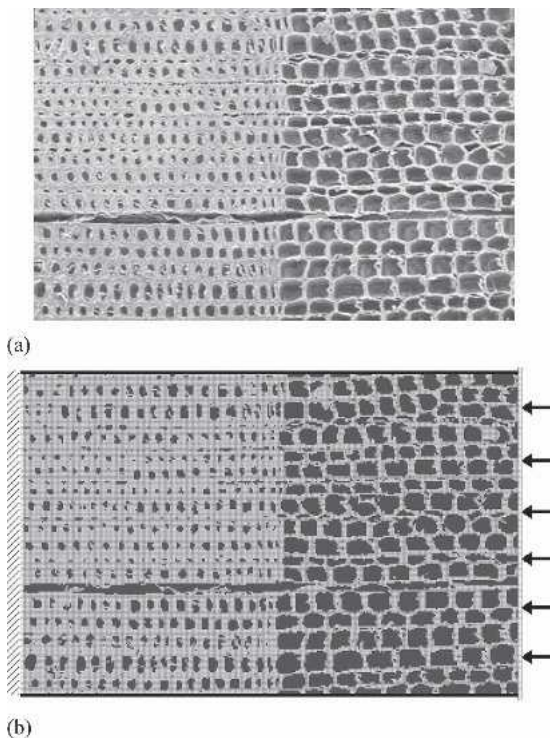


FIG. 2. A. SEM micrograph of uncompresssed mature loblolly pine (from Kultikova 1999). The micrograph images and area of 0.832×0.541 mm. B. MPM discretization of the image using 150×97 elements or $300 \times 194 = 58,020$ potential locations for particles.

($\rho/\rho_w = 0.791$) in the latewood region. This bulk density is higher than reported in Kultikova (1999) of 570 kg/m^3 , which is either a consequence of the resolution of the image, the specific region in the image, the actual value for cell-wall density, or an effect on cell-wall appearance caused by surface preparation for the SEM micrograph. The goal of this paper is to demonstrate MPM modeling, and thus the precise density was not crucial.

To simulate cell collapse by plastic deformation, the cell-wall material was assumed to be elastic-plastic (using a standard non-hardening, plasticity flow model for material modeling) with yielding occurring when the von-Mises stress reaches a critical value. In two-dimensional calculations (with the x - y plane being the transverse plane of analysis), the von-Mises criterion is

$$\frac{1}{2} [(\sigma_{xx} - \sigma_{yy})^2 + (\sigma_{xx} - \sigma_{zz})^2 + (\sigma_{zz} - \sigma_{yy})^2 + 6\tau_{xy}^2] \leq \sigma_Y^2 \quad (1)$$

For plane stress analysis, $\sigma_{zz} = 0$ and the material property σ_Y corresponds to the yield stress under uniaxial tension (yielding when $\sigma_{xx} = \sigma_Y$). For plane strain analysis, $\sigma_{zz} = \nu(\sigma_{xx} + \sigma_{yy})$ and the yield criterion is modified to:

$$(\sigma_{xx}^2 + \sigma_{yy}^2)(1 - \nu - \nu^2) - \sigma_{xx}\sigma_{yy}(1 + 2\nu - 2\nu^2) + 6\tau_{xy}^2 \leq \sigma_Y^2 \quad (2)$$

Under plain strain conditions, uniaxial tension will result in yielding when

$$\sigma_{xx} = \frac{\sigma_Y}{\sqrt{1 - \nu + \nu^2}} \quad (3)$$

For $\nu = 0.33$, the effective axial yield stress is equal to $1.133\sigma_Y$. The work of Tabarsa (1999; Tabarsa and Chui 2000, 2001) estimated axial yield stresses of 431 MPa for white spruce and 474 MPa for jack pine. Here the yield stress was varied from $\sigma_Y = 100$ MPa to very high values (to simulate an elastic response). Most calculations used $\sigma_Y = 500$ MPa. The convergence tests used plane stress conditions, but all other calculations used plain strain conditions.

The boundary conditions for radial compression are illustrated in Fig. 2B. The right side of the specimen was compressed at a constant rate by a rigid piston. The left side of the specimen was restrained with zero-displacement boundary conditions. The top and bottom of the specimen were restrained by rigid particles to confine compression to the axial direction. To monitor axial stress on the wood, a layer of particles was inserted between the wood material and the zero-displacement boundary condition on the left edge. The applied stress was calculated from the average stress in these particles. The modulus and density of the extra particles were very high such that their deformation was negligible during the analysis. For transverse loading the piston was moved to the top, the lateral walls were moved to the left and right edges, and the zero-displacement boundary conditions and high-modulus particles were moved to the bottom.

All calculations were done using two-dimensional, explicit MPM code (Nairn 2005a). This serial code was run on single-processor, Linux cluster nodes ranging from 1.4 GHz to 2.8 GHz processor speeds. In explicit code, the time step is limited to $t_{step} \leq d/c_s$ where d is the minimal dimension of the elements in the background grid and c_s is the wave speed of the cell-wall material. The longitudinal wave speed of the assumed cell-wall material was $c_s = \sqrt{E/\rho} = 2665 \text{ m/s}$ and typical element dimensions were $d = 5$ microns. Typical time steps were therefore on the order 2×10^{-6} msec. These small time steps precluded simulations at typical loading rates used in quasi-static compression experiments. Work on compression of foam, however, shows that quasi-static results can be obtained provided the loading rate is lower than about 3% of the wave speed of the material (Bardenhagen et al. 2005). Some results below show slightly slower speeds are needed for elastic-plastic wood specimens.

RESULTS AND DISCUSSION

Convergence

Figure 3 shows results of transverse compression in the radial direction on the specimen in

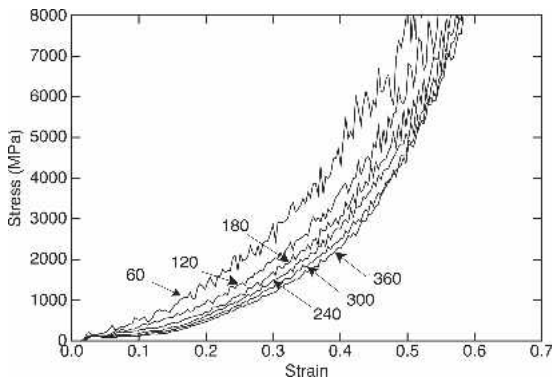


FIG. 3. Radial compression of loblolly pine, assuming the cell walls are linear elastic, as a function of resolution of the MPM model. The numbers indicate the number of particles in the horizontal direction across the wood specimen.

Fig. 2B compressed at 50 m/s (1.88% of wave speed) to compression strain of 0.6. These calculations used linear elastic cell-wall properties and varied the total number of particle positions in the horizontal direction. The results are resolution dependent for crude meshes (less than 200 particles), but converge for fine meshes (more than 300 particles). The maximum resolution used, or 360, exactly matched the number of pixels in the image. All subsequent calculations for this specimen used 300 particles as a compromise between adequate convergences and calculation speed. The convergence simulations were repeated for elastic-plastic cell-wall material with $\sigma_Y = 500$ MPa (results not shown); again a resolution of 300 particles was found to be adequate.

Both the elastic simulations (Fig. 3) and the elastic-plastic simulations had cell-wall collapse. The elastic material had elastic buckling, while the elastic-plastic material had plastic collapse of the cell walls. The plastic collapse occurred at lower stress than the elastic buckling. Experimental observations suggest that plastic collapse is the dominant mechanism in compression failure (Tabarsa and Chui 2000); thus the simulations in this paper focused on elastic-plastic material properties. There was little evidence of dynamic effects in the elastic results indicating that 50 m/s (1.88% of wave speed) was sufficiently slow for quasi-static results in

agreement with elastic foam results in Bardenhagen et al. 2005. In contrast, dynamic effects, as evidenced by oscillations at early times, were apparent of the elastic-plastic simulations (see 50 m/s curve in Fig. 4 below). These increased dynamics effects were probably due to slower plastic wave speeds (Kolsky 1963).

Radial compression in softwood

Figure 4 shows the results of radial compression at various speeds for the specimen in Fig. 2B using elastic-plastic cell-wall properties with $\sigma_Y = 500$ MPa. Dynamic effects were large for loading speed of 50 m/s (1.88% of wave speed) but were greatly reduced for loading speed of 25 m/s (0.94% of wave speed). For all speeds less than 10 m/s (0.38% of wave speed), dynamic effects were absent and the results were judged to be representative of quasi-static loading. The slowest loading speed of 1 m/s showed differences at high compression strain, but these may be a consequence of round-off error because those calculations required 5 to 10 times more time steps to reach high compression strain. All subsequent calculations used a loading rate of 10 m/s (0.38% of wave speed) to obtain results as quickly as possible but still within the range of quasi-static loading.

Figure 5 shows the results of radial compression at 10 m/s using elastic-plastic cell-wall properties with $\sigma_Y = 100$ MPa, 500 MPa, or

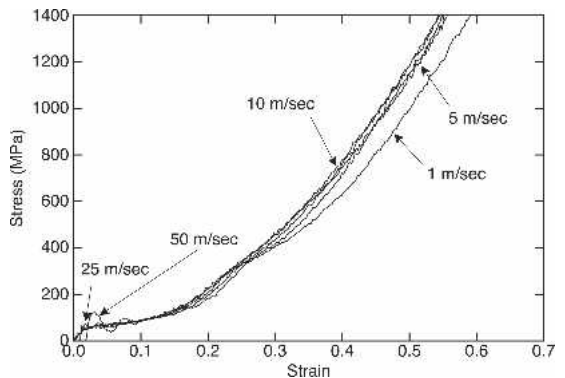


FIG. 4. MPM simulations of radial compression in loblolly pine using elastic-plastic cell properties ($\sigma_Y = 500$ MPa) as a function of the loading rate.

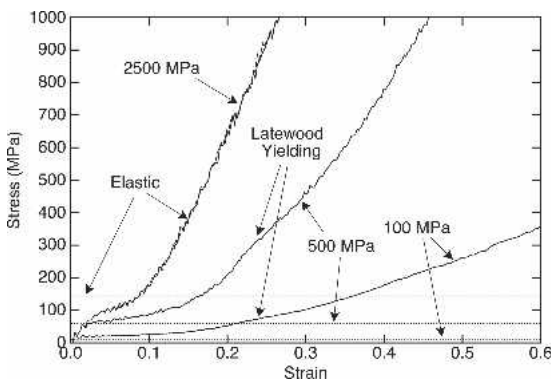


FIG. 5. MPM simulations of radial compression in loblolly pine using elastic-plastic cell properties with various yield stresses and for linear-elastic cell-wall properties. The linear-elastic results and $\sigma_Y = 2500$ MPa results are nearly identical and thus indistinguishable in the figure. The dotted horizontal lines are predictions of elastic buckling stress and plastic buckling stress (for $\sigma_Y = 500$ MPa or 100 MPa using foam theory). "Latewood Yielding" indicates onset of yielding in latewood cells.

2500 MPa, and for linear elastic cell-wall properties. There were few differences between the elastic results and the $\sigma_Y = 2500$ MPa results (the two curves superpose in Fig. 5) indicating that a yield stress of 2500 MPa was sufficiently high such that cell collapse was by elastic, rather than plastic buckling. For yield stress lower than about 1000 MPa, the dominant failure mode was plastic collapse. The stress at which plastic collapse occurred was approximately proportional to yield stress.

To show wood densification, Fig. 6 has snapshots of the geometry at various compressive strains for a yield stress of $\sigma_Y = 500$ MPa. At $\epsilon = 0.048$, the stress-strain curve was at the onset of plastic collapse and plastic energy can be seen within the earlywood zone with more yielding closer to the loading piston. As observed experimentally, cell collapse in radial loading occurs in earlywood (Bodig 1965; Tabarsa and Chui 2000) at cell walls under the highest stress (i.e., the thinnest cell walls in load-bearing paths). The results at $\epsilon = 0.168$ were at the beginning of densification. All yielding was still confined to the earlywood zone. At $\epsilon = 0.24$, there was a secondary yield point (see "Latewood Yielding"

humps in curves in Fig. 5) corresponding to the onset of plastic collapse in the latewood zone. Figure 6 shows plastic yielding spreading throughout the latewood at $\epsilon = 0.288$ (slightly beyond the $\epsilon = 0.24$ hump). Finally, higher strains ($\epsilon = 0.457$ and 0.600) showed continued yielding and densification. Thus MPM simulations are capable of tracking the structure of wood from plastic collapse and well into the densification zone. Although no microscopy of the densification of this specific specimen was available, the structure of collapsed and densified wood was very similar to images of compressed wood (Kultikova 1999).

Tangential compression in softwood

The compression simulations were repeated for tangential compression by loading in the vertical direction. The results as a function of rate were analogous to the radial results (see Fig. 4) and are not repeated here. Figure 7 shows the results of tangential compression at 10 m/s using elastic-plastic cell-wall properties with $\sigma_Y = 100$ MPa, 500 MPa, or 2500 MPa, and for linear elastic cell-wall properties. There were few differences between the elastic results and the $\sigma_Y = 2500$ MPa results, indicating that that yield stress was sufficiently high that deformation was dominated by elastic processes. For yield stresses lower than about 1000 MPa, the dominant failure modes were plastic collapse followed by densification. The plastic collapse occurred throughout the specimen. When compared to radial loading (see radial results for $\sigma_Y = 500$ MPa repeated from Fig. 5 for comparison), the plastic collapse in tangential loading required higher loads because it involved thick-walled latewood cells rather than being confined to thin-walled, earlywood cells. Furthermore, the second plastic collapse in the radial compression at a strain of 0.24 caused by the onset of latewood plastic collapse is not seen in tangential compression because that mechanism was not present. Once both earlywood and latewood plastic collapse has occurred (for strains above about 0.26), the stresses during remaining den-

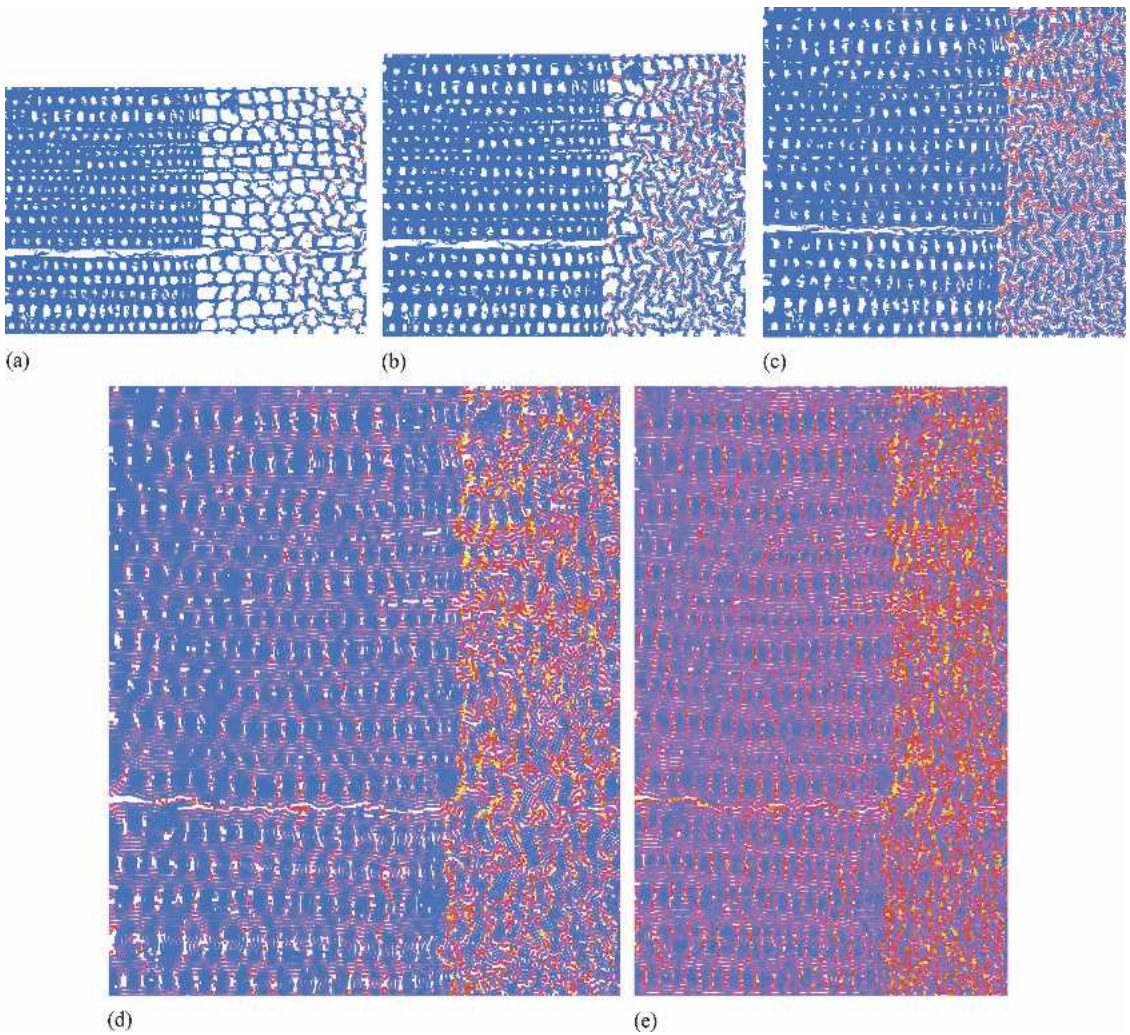


FIG. 6. Wood structure during radial compression as a function of applied compressive strain, ϵ . A. $\epsilon = 0.048$. B. $\epsilon = 0.168$. C. $\epsilon = 0.288$. D. $\epsilon = 0.457$. E. $\epsilon = 0.600$. The colors indicate cumulative plastic energy dissipation with blue zones indicating zero plastic work to red zones and lighter colors with high plastic energy.

sification were similar for radial and tangential compression. These results agree with experimental observations on softwood with distinct earlywood and latewood zones (Bodig 1963). The interpretation is that the latewood zones act as columns of reinforcement during tangential loading that increase both stiffness and plastic collapse stress (Bodig 1963).

Figure 8 has snapshots of tangential densification at various compressive strains for a yield

stress of $\sigma_y = 500$ MPa. In contrast to radial compression, plastic collapse occurs simultaneously in earlywood and latewood as shown when $\epsilon = 0.186$. At higher strains there is continued densification. In addition, the latewood material moves into the earlywood zone, thus compressing that zone in two directions. Again, MPM simulations are capable of tracking the structure of wood from plastic collapse through to densification.

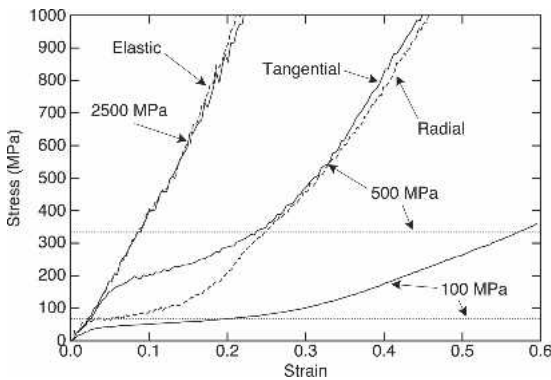


Fig. 7. MPM simulations of tangential compression in loblolly pine using elastic-plastic cell properties with various yield stresses and for linear-elastic cell-wall properties. The dotted horizontal lines are predictions of plastic buckling using foam theory.

Radial and tangential compression in hardwood

Hardwoods differ from softwoods in their anatomy and therefore have differences in compression properties. For example, hardwoods have wider ray cells in the radial direction (Haygreen and Bowyer 1996) that can reinforce radial compression. Hardwoods also have vessel elements or pores (Haygreen and Bowyer 1996) that should influence compression and densification. To investigate the effects of hardwood anatomy, compression simulations were done on mature yellow poplar (*Liriodendron tulipifera*)—a diffuse porous hardwood. Figure 9A shows an SEM micrograph of uncompressed yellow poplar (Kultikova 1999). The resolution of the image, as obtained, was 497×325 pixels and it images an area of 0.802×0.524 mm. This image was converted to a bitmap file and then mapped to a background grid for the image of 150×98 elements. This background grid provides for $300 \times 196 = 58,800$ potential locations for particles. The MPM model had 33,084 particles for a bulk density of 844 kg/m^3 ($\rho/\rho_w = 0.563$) compared to the reported density of 610 kg/m^3 (Kultikova 1999). Higher resolution images with attention to surface preparation and digitization may be needed for more accurate MPM model construction.

The MPM model for the specimen in Fig. 9A was subjected to radial and tangential compression at 10 m/s using elastic-plastic cell-wall properties with $\sigma_y = 500$ MPa. Figures 9B (radial loading) and 9C (tangential loading) illustrate load-carrying paths or magnitude of the stress in the direction of loading. Clearly the ray cells bear load that reinforced this hardwood during radial compression. There were fewer and less organized load-bearing paths during tangential loading. Figure 10 shows stress-strain curves for radial and tangential compression. In this hardwood, the radial direction was stiffer and required higher loads for buckling than the tangential direction. These results are the reverse of the softwood results. Experimental observations typically show that softwoods are stiffer and have higher plateau stress in the tangential direction while hardwoods are similar in the tangential and radial directions or are stiffer with higher plateau stress in radial compression (Bodig 1965). MPM simulations agree with these observations with Fig. 9B providing visualization of reinforcement by the ray cells.

Larger, lower density specimen

One final, and largest calculation, was done for ponderosa pine (*Pinus ponderosa*) in tangential loading. An image was scanned from a figure in Haygreen and Bowyer 1996. The unstrained, digitized MPM model is shown in Fig. 11A. The image covers an area approximately 1.00×1.29 mm. The mesh behind the image had 200×258 elements or $400 \times 516 = 206,400$ particle locations. The MPM model had 76,242 particles for a bulk density of 554 kg/m^3 ($\rho/\rho_w = 0.369$) that is closer to the density of many woods and lower than in other calculations. An MPM simulation was done for loading in the tangential direction at 10 m/s and having $\sigma_y = 500$ MPa. Figure 11B shows the specimen at $\epsilon = 0.186$, which is near the middle of the post-buckling, plateau region. The initial damage was concentrated around the resin canal near the bottom of the specimen. Many regions of earlywood cells, particularly those with thin walls, have collapsed. The latewood zone has under-

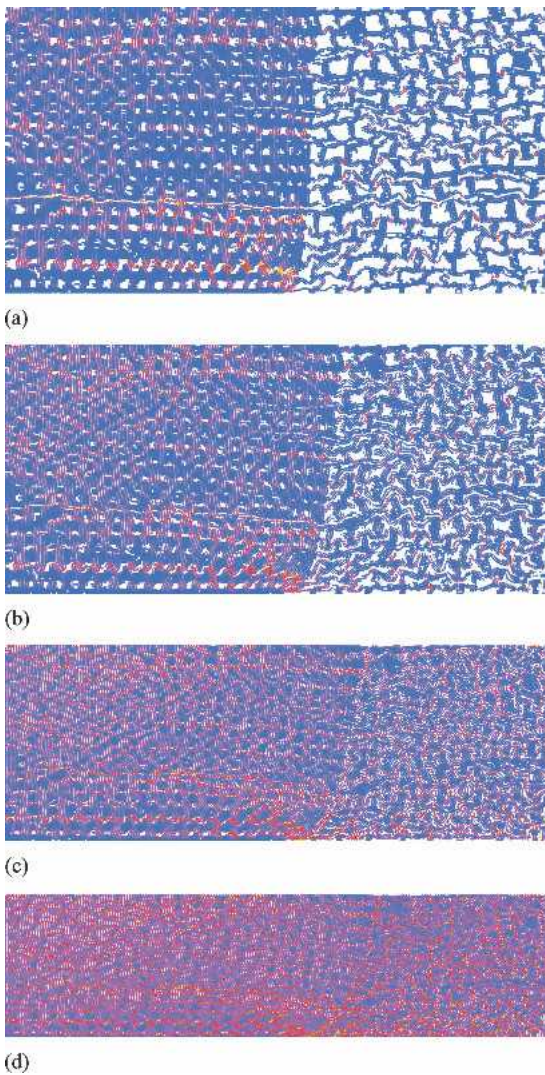


FIG. 8. Wood structure during tangential compression as a function of applied compressive strain, ϵ . A. $\epsilon = 0.146$. B. $\epsilon = 0.297$. C. $\epsilon = 0.446$. D. $\epsilon = 0.595$. The colors indicate cumulative plastic energy dissipation with blue zones indicating zero plastic work to red zones and lighter colors with high plastic energy.

gone macroscopic buckling. The compressive stress-strain curve for this specimen is shown in Fig. 10. The results were similar to other results except at lower stresses due to the lower density.

Mechanical properties

Figure 1 shows key features of transverse compression in wood including the initial elastic

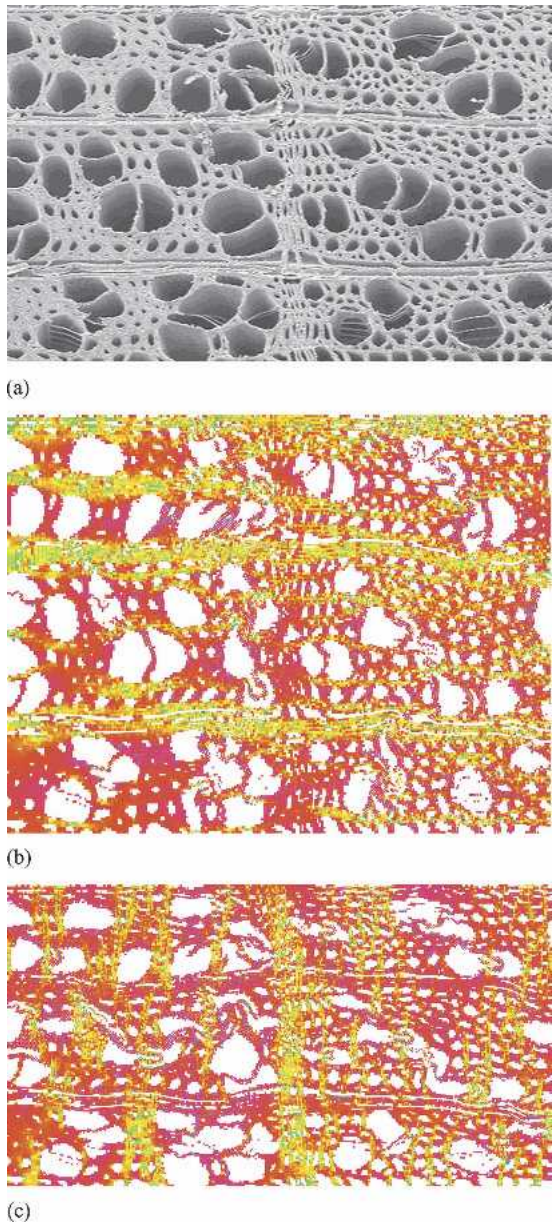


FIG. 9. A. SEM micrograph of uncompressed mature yellow poplar (from Kultikova 1999). The micrograph images an area of 0.802×0.524 mm. B. MPM results in radial compression at $\epsilon = 0.150$. C. MPM results in tangential compression at $\epsilon = 0.153$. The colors indicate stress in the direction of loading with green and lighter colors indicating more compression.

modulus (slope of the initial linear portion of the curve), onset of yielding by plastic (or elastic) buckling at a stress σ_b (and strain ϵ_b), and start

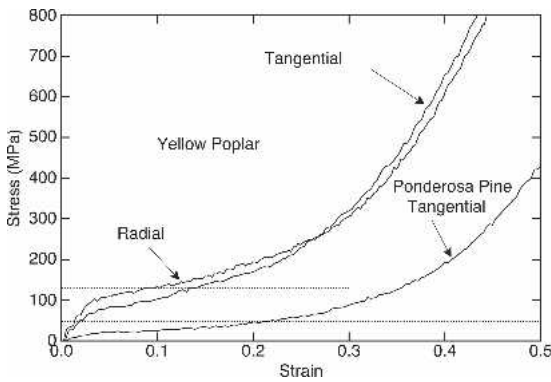


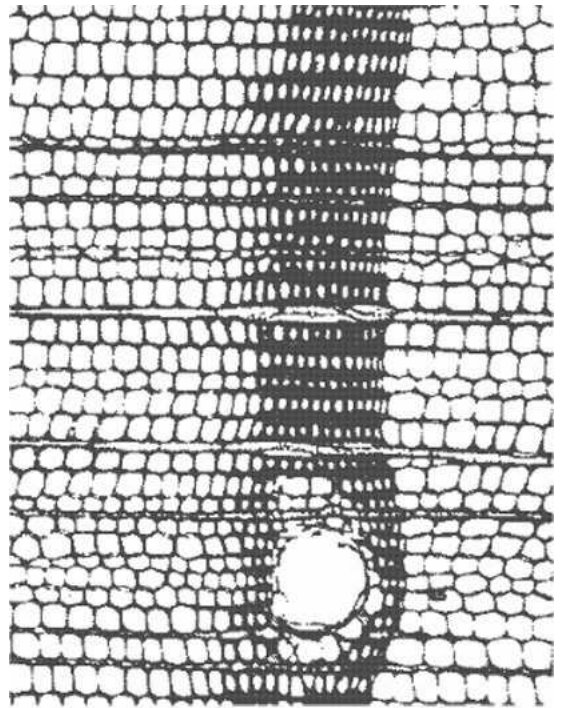
FIG. 10. MPM simulations of radial and tangential compression of yellow poplar and for tangential compression of ponderosa pine. The calculations used elastic-plastic cell properties with $\sigma_y = 500$ MPa. The dotted horizontal lines are predictions of plastic buckling using foam theory.

of densification at defined stress σ_d (and strain ϵ_d). Table 1 has the results of extracting the key features from each of the simulation results as a function of the assumed yield stress or for an elastic material (∞ yield stress). For loblolly pine, the initial modulus was slightly higher in tangential loading compared to radial loading due to reinforcement effect of the latewood region during tangential loading. The separate earlywood and latewood moduli (E_{early} and E_{late}) were estimated by equating the radial and tangential moduli to transverse (series) and axial (parallel) moduli of a unidirectional composite (where the latewood plays the role of the fiber reinforcement) (Jones 1975). The results are

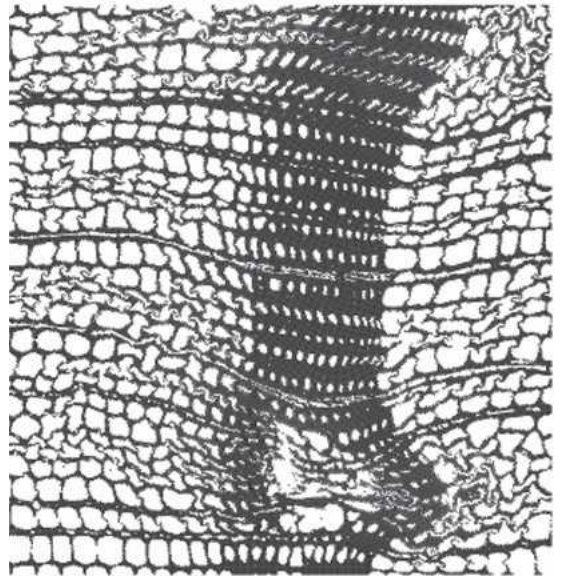
$$\frac{1}{E_{radial}} = \frac{1}{2740} = \frac{V_{early}}{E_{early}} + \frac{V_{late}}{E_{late}} \quad (4)$$

$$E_{tangential} = 3252 = V_{early}E_{early} + V_{late}E_{late} \quad (5)$$

where V_{early} and V_{late} are volume fractions of the early and latewood regions. Evaluating $V_{early} = 0.473$ and $V_{late} = 0.527$ (see Fig. 2) and solving gives $E_{early} = 1919$ MPa and $E_{late} = 4449$ MPa. The situation for yellow-poplar is reversed. For that hardwood, the wider ray cells reinforced the radial loading resulting in slightly higher modulus in radial loading than in tangen-



(a)



(b)

FIG. 11. Wood structure in an MPM model of ponderosa pine. A. The unstrained state. B. After tangential compression to $\epsilon = 0.186$.

TABLE 1. Evaluation of initial modulus (E), stress and strain for the onset of buckling (σ_b and ϵ_b) and the stress and strain for the onset of densification (σ_d and ϵ_d) from the MPM simulations as a function of assumed yield stress (∞ yield stress indicates elastic material). The "Elastic Loading" region (see Fig. 1) and the buckling and densification stresses and strains are illustrated in Fig. 1; the modulus is the slope of the "Elastic Loading" region.

Species	Direction	σ_Y (MPa)	E (MPa)	σ_b (MPa)	ϵ_b	σ_d (MPa)	ϵ_d
Loblolly pine	Radial	100	2740	16.7	0.43%	40.0	24.8%
Loblolly pine	Radial	500	2740	54.2	1.80%	161.4	27.1%
Loblolly pine	Radial	2500	2740	90.7	3.13%	238.4	27.7%
Loblolly pine	Radial	∞	2740	92.6	3.20%	213.4	28.1%
Loblolly pine	Tangential	100	3252	39.1	1.32%	79.9	29.9%
Loblolly pine	Tangential	500	3252	173.6	5.45%	330.4	29.5%
Loblolly pine	Tangential	2500	3252	—	—	—	—
Loblolly pine	Tangential	∞	3252	—	—	—	—
Yellow poplar	Radial	500	3731	102.1	2.75%	221.1	31.4%
Yellow poplar	Tangential	500	2479	71.4	2.75%	192.4	30.7%
Ponderosa pine	Tangential	500	648	15.2	2.47%	63.8	36.2%

tial loading. The modulus for ponderosa pine was lower due to its lower density.

The onset of buckling scales with σ_Y for $\sigma_Y = 100$ and $\sigma_Y = 500$ MPa indicating that the predominant failure mechanism was by plastic buckling of cell walls. Plots of plastic energy (see Figs. 6 and 8) confirm this observation. The buckling load for ponderosa pine was lower because the lower density resulted in thinner cell walls that buckled at lower loads. The buckling for $\sigma_Y = 2500$ MPa and for elastic properties were indistinguishable for radial compression and difficult to detect for tangential loading. The initiation of failure in these two simulations was thus by elastic buckling. Observations of real wood (Tabarsa 1999; Tabarsa and Chui 2000, 2001) suggest that plastic buckling is the predominant failure mechanism; thus the lower yield stress results are more representative of actual wood compression.

The method used to identify densification strain (see Fig. 1) gave results that were independent of loading direction and increased with the total free-volume in the undeformed state. The loblolly pine simulation had 39.3% free volume and densification began at an average $\epsilon_d = 27.5\%$. The yellow-poplar simulation had slightly more free volume (43.7%) and a slightly higher average $\epsilon_d = 31.5\%$. Finally, the lowest density ponderosa pine had 63.1% free volume and the highest $\epsilon_d = 36.2\%$.

Comparison to foam theory

Gibson et al. 1982, calculated the initial modulus and the elastic and plastic buckling stresses for a 2D foam modeled as a regular array of hexagonal cells as a function of t , l , and θ (see Fig. 1). For a symmetric hexagonal array ($\theta = 30^\circ$), the results are

$$E = \frac{4E_w}{\sqrt{3}} \left(\frac{t}{l} \right)^3$$

$$\sigma_b \text{ (elastic)} = \frac{E}{10}$$

$$\sigma_b \text{ (plastic)} = \frac{2\sigma_Y}{3} \left(\frac{t}{l} \right)^3 \quad (6)$$

For a regular hexagonal array, Gibson et al. 1982, further calculated the key thickness ratio to be

$$\frac{t}{l} = \frac{\sqrt{3}}{2} \frac{\rho}{\rho_w} \quad (7)$$

This theory was derived for low-density foams (ρ/ρ_w , $t/l \ll 1$) because the deformation was assumed to be predominantly bending of wall elements and the thickness ratio assumes thin walls. Because the calculations in this paper, and most real wood, have moderate density, it is useful to generalize the thickness ratio calculation to one that works at any foam density:

$$\frac{t}{l} = \sqrt{3} \left(1 - \sqrt{1 - \frac{\rho}{\rho_w}} \right) \quad (8)$$

Comparison of Eq. (8) to Eq. (7) shows that the low-density result is within 5% for $\rho/\rho_w < 0.2$ but is off by more the 20% for $\rho/\rho_w > 0.64$. The calculations in this paper used the more accurate result in Eq. (8). Note that although this approach improved the calculation of t/l , the mechanical property equations are still based on low-density foams and will lose accuracy as t/l increases. Nevertheless, it is useful to compare predictions to simulations to assess both the simulations and the accuracy of foam theory.

Foam theory calculations, with MPM results in parentheses, are given in Table 2. All foam theory calculations are consistent with MPM simulations indicating the numerical modeling derived reasonable results. The MPM results, however, are expected to be more accurate because they model the entire structure and make no approximations about deformation mechanisms or density. All foam theory moduli are too high except for radial loading of loblolly pine. The tangential modulus has the largest error, which is due to the assumption of deformation only by bending. Bending deformation scales as the cube of the thickness of the walls (Gibson et al. 1982). As the walls get thicker, the bending stiffness gets large and the calculation needs to account for axial deformation as well. The error in the foam theory is a consequence of ignoring this axial deformation. The foam theory modulus in the radial direction is too low because it fails to account for files of radial cells that pro-

vide a straight path for bearing axial load (see Fig. 2). In contrast, the cells in a regular hexagonal array alternate and disrupt radial load-bearing paths. The load-bearing paths in loblolly pine can be confirmed in the MPM results by plotting stress in the loading direction prior to buckling.

The foam theory elastic and plastic buckling loads are shown as dotted horizontal lines in Figs. 4, 7, and 10. In general, foam theory overestimates the stress at the onset of plastic buckling. In real wood, the initiation of buckling will occur at imperfections or where the cell walls are thin and the stress is high. Foam theory, however, assumes a regular array and can not model variations in wood anatomy. The one exception was for radial loading of loblolly pine at low yield stress where the foam theory prediction was lower than numerical results. This simulation, however, had very little elastic deformation, which made it difficult to precisely determine the onset of buckling. The trends of all other results are more representative and suggest that failure modeling of wood that is influenced by wood anatomy requires full modeling of real-wood morphology. Models based on idealized structures and regular arrays are of limited use.

Limitations

MPM simulations of deformation in wood were found to be a useful tool for numerical modeling of realistic wood structures. This section discusses some limitations of the results. The calculations were not small. Typical calcu-

TABLE 2. Comparison of foam theory predictions for initial modulus (E) and for elastic and plastic buckling stress (σ_b) to MPM results as a function of assumed yield stress. The numbers are foam theory calculations, the numbers in parentheses are the MPM results.

Species	Direction/wood	σ_y (MPa)	E (MPa)	σ_b (MPa) (elastic)	σ_b (MPa) (plastic)
Loblolly pine	Radial/early	100	1510 (1919)	144 (-)	11.8 (16.7)
Loblolly pine	Radial/early	500	1510 (1919)	144 (-)	58.8 (54.2)
Loblolly pine	Radial/early	2500	1510 (1919)	144 (90.7)	294 (-)
Loblolly pine	Radial/late	100	20390 (4449)	1942 (-)	66.7 (39.1)
Loblolly pine	Radial/late	500	20390 (4449)	1942 (-)	333.3 (173.6)
Loblolly pine	Radial/late	2500	20390 (4449)	1942 (-)	1667 (-)
Yellow poplar	Average/bulk	500	4965 (3105)	473 (-)	130 (86.8)
Ponderosa pine	Tangential/bulk	500	1111 (648)	106 (-)	47.9 (15.2)

lations to 60% compression strain required 4 to 100 hours (depending on processor speed and load). The longest calculations (for loading at 1 m/s) took 13 days. But, these calculations were done with explicit, serial code. MPM is readily amenable to an implicit algorithm (Guilkey and Weiss 2003), which would permit longer time steps, and to massive parallelization (Parker 2002). It is expected the calculations could be sped up by an factor at least 10,000. A factor of 100 is already available as demonstrated by 3D foam calculations with 8,000,000 particles on 48 processors completing in times similar to the calculations in this paper (Brydon and Bardenhagen 2005). An increase in efficiency or a restriction to small strains could be exploited for some combination of larger calculations, slower loading speeds, or extension into realistic, three-dimensional wood structures.

Most calculations had MPM models with densities higher than typical wood. As a consequence, the stiffness and failure loads are higher than typical experimental results. For direct comparison between MPM results and experiments, it will be important to match the density of the wood to the density of the numerical calculations. More realistic density is easily modeled by using high-resolution microscopy with properly prepared surfaces coupled with careful mapping of the intensity of the images into cell-wall material. There are no problems associated with MPM modeling at any density.

Finally, there are three areas where MPM code development would increase the realism and accuracy of the simulations. First, these calculations used conventional MPM methods. The recently derived generalized MPM (GIMP) provides tools for modifying shape functions that improves accuracy at large deformations (Bardenhagen and Kober 2004). Second, although MPM automatically handles contact between cell walls and permits calculations to high densification, the physics of this automatic contact is by stick boundary conditions. These conditions are probably adequate for modeling of compression, but might lack realism for future work such as numerical modeling of the mechanical properties wood *after* densification

(Kultikova 1999). Alternate contact methods in MPM are available for modeling frictional sliding between different objects (Bardenhagen et al. 2000, 2001) or across crack surfaces (Nairn 2003), but contact between cell walls in wood or foam is *self contact* within the same object. Implementing self contact would be a valuable addition to MPM. Third, the simulations might be improved with altered boundary conditions. The simulations here used a rigid wall on both sides of the specimen. This wall confined the specimen and gave very stable results. The results are appropriate for compression of specimens restrained on the edges. Altered boundary conditions, such as flexible walls or wall properties based on bulk specimen properties, might be important for analysis of other loading configurations.

CONCLUSIONS AND FUTURE WORK

A major drawback to numerical modeling of wood in the past has been the ability of various methods to deal with actual wood structures. This paper has demonstrated that the material point method (MPM) can handle large-scale, morphology-based models of real wood. It is easy to discretize a micrograph of wood into an MPM model. Once discretized the MPM calculations are very stable, can be carried out to large deformations, can include elastic-plastic properties, and can automatically model contact between cell walls. This capability was used here to study transverse compression in wood. It was possible to identify key effects of wood anatomy that explain differences between radial loading and tangential loading and between wood species. The results were compared to foam theory. Although foam theory captures some key deformation mechanisms in transverse properties of wood, it is not capable of analyzing more complex phenomena associated with variable wood anatomy.

Some potential applications for MPM modeling of realistic wood structures are:

- Direct comparison of experimental observations of failure in wood coupled with MPM

modeling of the morphology of the specimen: MPM modeling could be used to interpret experimental results, to extract material properties of cell walls, and to develop new failure models for wood. This work is not limited to compression loading; it could model any loading conditions.

- Extension to realistic three-dimension models of wood: X-ray tomography methods should be able to resolve slices of wood specimens (Smith et al. 2001). Each slice could be digitized into a plane of the model analogous to the methods used here for a single 2D image. A collection of slices would automatically be assembled into a valid 3D model. Unlike FEA meshes, where connectivity between slices would be difficult, assignment of material points within a 3D grid from tomography data would be sufficient to fully define the 3D structure (Brydon et al. 2005). 3D models could be used to study the effect of three-dimensional variations in wood anatomy.
- Modeling of the processing of wood-based composites: One area of MPM research is developing capabilities for simulations with fluid-structure interactions (Guilkey et al. 2003). This capability could be used to model processing of wood-based composites including interactions between adhesives and wood and compression of wood phases within the composite. MPM modeling can easily accommodate moisture- and temperature-dependent constitutive laws for the wood.
- Modeling of drying processes in wood: Another MPM development has demonstrated coupled dynamic mechanics and diffusion calculations (Nairn 2005b). This capability could be used to study the effect of 2D and 3D variations in wood anatomy on the wood-drying process. Coupling the drying process to mechanics calculations and MPM fracture algorithms (Nairn 2003) might be able to model cracking during drying.

ACKNOWLEDGMENTS

The work was supported by a grant from the Department of Energy DE-FG03-02ER45914

and by the University of Utah Center for the Simulation of Accidental Fires and Explosions (C-SAFE), funded by the Department of Energy, Lawrence Livermore National Laboratory, under Subcontract B341493. I also thank S. G. Bardenhagen and A. D. Brydon (Los Alamos National Lab) for many useful discussions.

REFERENCES

- ATLURI, S. N., AND S. P. SHEN. 2002. The meshless local Petrov-Galerkin (MLPG) method. Tech. Science Press, Forsyth, GA.
- BARDENHAGEN, S. G., AND E. M. KOBER. 2004. The generalized interpolation material point method. *Computer Modeling Eng. & Sci.* B:477–496.
- , J. U. BRACKBILL, AND D. SULSKY. 2000. The material point method for granular materials. *Computer Methods Appl. Mech. Eng.* 187:529–541.
- , J. E. GUILKEY, K. M. ROESSIG, J. U. BRACKBILL, W. M. WITZEL, AND J. C. FOSTER. 2001. An improved contact algorithm for the material point method and application to stress propagation in granular materials. *Computer Modeling Eng. Sci.* 2:509–522.
- , A. D. BRYDON, AND J. E. GUILKEY. 2005. Insight into the physics of foam densification via numerical simulation. *J. Mech. Phys. Solids.* 53:597–617.
- BELYTSCHKO, T., Y. Y. LU, AND L. GU. 1994. Element-free Galerkin methods. *Int. J. Num. Meth. Eng.* 37:229–256.
- BODIG, J. 1963. The peculiarity of compression of conifers in radial direction. *Forest Prod. J.*, 13:438.
- . 1965. The effect of anatomy on the initial stress-strain relationship in transverse compression. *Forest Prod. J.* 15:197–202.
- . 1966. Stress-strain relationship for wood in transverse compression. *J. Materials* 1:645–666.
- , AND B. A. JAYNE. 1982. *Mechanics of wood and wood composites.* Van Nostran-Reinhold Co, Inc., New York, NY.
- BOURKE, P. 2004. BMP file format. <http://astronomy.swin.edu.au/~pbourke/dataformats/bmp/>.
- BRYDON, A., AND S. BARDENHAGEN. 2005. Personal communication.
- , ———, E. A. MILLER, AND G. T. SEIDLER. 2005. Simulation of the densification of real open cell foam microstructures. *J. Mech. Phys. Solids.* 53:2638–2660.
- DAVIDS, W. G., E. N. LANDIS, AND S. VASIC. 2003. Lattice models for the prediction of load-induced failure and damage in wood. *Wood Fiber Sci.* 35:120–134.
- EASTERLING, K. E., R. HARRYSSON, L. J. GIBSON, AND M. F. ASHBY. 1982. On the mechanics of balsa and other woods. *Proc. Royal Soc. Lond. A.* 383:31–41.
- GIBSON, L. J., AND M. F. ASHBY. 1997. *Cellular solids: Structure and properties.* Cambridge University Press, UK.
- , K. E. EASTERLING, AND M. F. ASHBY. 1981. The

- structure and mechanics of cork. *Proc. Royal Soc. Lond. A.* 377:99–117.
- , M. F. ASHBY, G. S. SCHAJER, AND C. I. ROBERTSON. 1982. The mechanics of two-dimensional cellular materials. *Proc. Royal Soc. Lond. A.* 382:25–42.
- GUILKEY, J. E., AND J. A. WEISS. 2003. Implicit time integration for the material point method: quantitative and algorithmic comparisons with the finite element method. *Int. J. Num. Meth. Eng.* 57:1323–1338.
- , T. HARMON, B. KASHIWA, A. XIA, AND P. A. MCMURTRY. 2003. An Eulerian-Lagrangian approach for large deformation fluid-structure interaction problems, part 1: algorithm development. *Proc. 2nd Inter. Conf. on Fluid-Structure Interactions.* June 24–26, 2003, Cadiz, Spain.
- GUO, Y., AND J. A. NAIRN. 2004. Calculation of J-Integral and stress intensity factors using the material point method. *Computer Modeling Eng. Sci.* 6:295–308.
- HAYGREEN, J. G., AND J. L. BOWYER. 1996. *Forest products and wood science: An Introduction.* Iowa State University Press, Ames, IA.
- JONES, R. M. 1975. *Mechanics of composite materials.* Scripta Book Company, Washington, DC.
- KENNEDY, R. W. 1968. Wood in transverse compression. *Forest Prod. J.* 18:36–40.
- KOLSKY, H. 1963. *Stress waves in solids.* Dover, New York, NY.
- KULTIKOVA, E. V. 1999. *Structure and properties relationships of densified wood.* M.S. Thesis, Wood Science and Forest Products, Virginia Polytechnic Institute and State University, Blacksburg, VA.
- KUNESH, R. H. 1968. Strength and elastic properties of wood in transverse compression. *Forest Prod. J.* 18:36–40.
- LANDIS, E. N., S. VASIC, W. G. DAVIDS, AND P. PARROD. 2002. Coupled experiments and simulations of microstructural damage in wood. *Exp. Mech.* 42:389–394.
- NAIRN, J. A. 2003. Material point method calculations with explicit cracks. *Computer Modeling Eng. Sci.* 4:649–664.
- . 2005a. Source code and documentation for NairnMPM Code for Material Point Calculations. <http://oregonstate.edu/~nairnj/>.
- . 2005b. Diffusion calculations in NairnMPM solid mechanics code. Unpublished results, see Nairn, 2005a for source code.
- PARKER, S. G. 2002. A component-based architecture for parallel multi-physics PDE simulation. *International Conference on Computational Science (ICCS2002) Workshop on PDE Software, April 21–24, 2002, Amsterdam, Netherlands.*
- PELLICANE, P. J., J. BODIG, AND A. L. MREMA. 1994a. Behavior of wood in transverse compression. *J. Testing Eval.* 22:383–387.
- , ———, AND ———. 1994b. Modeling wood in transverse compression. *J. Testing Eval.* 22:376–382.
- SHIARI, B., AND P. M. WILD. 2004. Finite element analysis of individual wood-pulp fibers subjected to transverse compression. *Wood Fiber Sci.* 36:135–142.
- SMITH, R. A., M. J. PAULUS, J. M. BRANNING, AND P. J. PHILLIPS. 2001. X-ray computed tomography on a cellular polysiloxane under compression. *J. Cellular Plastics* 37: 231–248.
- SMITH, I., E. LANDIS, AND E. GONG. 2003. *Fracture and fatigue in wood.* John Wiley & Sons, Ltd., New York, NY.
- SULSKY, D., AND H. K. SCHREYER. 1996. Axisymmetric form of the material point method with applications to upsetting and Taylor impact problems. *Computer Methods. Appl. Mech. Eng.* 139:409–429.
- , Z. CHEN, AND H. L. SCHREYER. 1994. A particle method for history-dependent materials. *Computer Methods Appl. Mech. Eng.* 118:179–186.
- , S.-J. ZHOU, AND H. L. SCHREYER. 1995. Application of a particle-in-cell method to solid mechanics. *Comput. Phys. Commun.* 87:236–252.
- TABARSA, T. 1999. *Compression perpendicular-to-grain behaviour of wood.* Ph.D. Thesis, Forestry and Environmental Management, The University of New Brunswick, Canada.
- , AND Y. H. CHUI. 2000. Stress-strain response of wood under radial compression. Part I. Test method and influences of cellular properties. *Wood Fiber Sci.* 32: 144–152.
- , AND ———. 2001. Characterizing microscopic behavior of wood under transverse compression. Part II. Effect of species and loading direction. *Wood Fiber Sci.* 33:223–232.
- ZHOU, S. 1998. *The numerical prediction of material failure based on the material point method.* Ph.D. Thesis, University of Mexico, Albuquerque, NM.
- ZHU, H. X., N. J. MILLS, AND J. F. KNOTT. 1997. Analysis of the Higher Strain Compression of Open Cell Foams. *J. Mech. Phys. Solids* 45:1875–1904.